Nuclear Engineering and Technology 53 (2021) 2708–2715

Contents lists available at ScienceDirect

Nuclear Engineering and Technology

journal homepage: www.elsevier.com/locate/net

Original Article

Position error compensation of the multi-purpose overload robot in nuclear power plants

Guodong Qin [a], Aihong Ji [a, *], Yong Cheng [b], Wenlong Zhao [b], Hongtao Pan [b], Shanshuang Shi [b, **], Yuntao Song [b]

[a] College of Mechanical & Electrical Engineering, Nanjing University of Aeronautics & Astronautics, Nanjing, 210016, China
[b] Institute of Plasma Physics, Chinese Academy of Science, Hefei, 230031, China

ARTICLE INFO

Article history:
Received 10 September 2020
Received in revised form
16 January 2021
Accepted 7 February 2021
Available online 15 February 2021

Keywords:
Multi-purpose overload robot
Remote handling system
Levenberg-marquardt
Parameter identification

ABSTRACT

The Multi-Purpose Overload Robot (CMOR) is a key subsystem of China Fusion Engineering Test Reactor (CFETR) remote handling system. Due to the long cantilever and large loads of the CMOR, it has a large rigid-flexible coupling deformation that results in a poor position accuracy of the end-effector. In this study, based on the Levenberg-Marquardt algorithm, the spatial grid, and the linearized variable load principle, a variable parameter compensation model was designed to identify the parameters of the CMOR's kinematics models under different loads and at different poses so as to improve the trajectory tracking accuracy. Finally, through Adams-MATLAB/Simulink, the trajectory tracking accuracy of the CMOR's rigid-flexible coupling model was analyzed, and the end position error exceeded 0.1 m. After the variable parameter compensation model, the average position error of the end-effector became less than 0.02 m, which provides a reference for CMOR error compensation.

1. Introduction

The Multi-purpose Overload Robot (CMOR) is a vital subsystem of the remote handling system of the China Fusion Engineering Test Reactor (CFETR) [1], as it can perform various vacuum indoor maintenance tasks, as shown in Fig. 1. While bearing a super large load of 2000 kg, the limitation of the device's structure size regarding the design space of the manipulator should also be considered. Generally, the CMOR's tasks include dust detection and removal in the vacuum chamber, vacuum chamber inspection, tritium retention monitoring, vacuum chamber diagnosis and maintenance, maintenance of the first wall cladding, and maintenance of the neutral beam casing bushing module [2]. With a long cantilever and a large load, the deformation error of the rigid and flexible coupling of the CMOR becomes relatively large [3–5]. In the static mechanical analysis of the CMOR under the cantilever state, when the end-effector was fully loaded (2000 kg), the flexible deformation was 77 mm without considering the control error of each joint [6]. In addition, due to the influence of the manufacturing error, machining error, controller control error, temperature field, magnetic field, etc., the trajectory tracking error of the CMOR's end-effector is significant, and the absolute positioning accuracy is low, which seriously affects the high-precision positioning and trajectory tracking operation of the CMOR. Thus, it would not be able to satisfy the commercial operation and maintenance efficiency of the fusion engineering test reactor in the future.

The CMOR's rigid-flexible coupling model is a complex nonlinear system with many dynamic parameters. Due to the lack of an accurate dynamic model, the artificial closed-loop mechanism (Man-in-the-loop) is often introduced into control systems to improve their position accuracy and the stability of their maintenance operations [7,8]. However, in the form of the master-slave teleoperation, low maintenance efficiency cannot meet the requirements of the future commercial operation of nuclear fusion power plants. Thus, efficient automatic maintenance is an inevitable trend [9].

Considering that the rigid and flexible coupling of the CMOR causes a large absolute position error to the end-effector, a simply

* Corresponding author.
** Corresponding author.
E-mail addresses: meeahji@nuaa.edu.cn (A. Ji), shiss@ipp.ac.cn (S. Shi).

https://doi.org/10.1016/j.net.2021.02.005

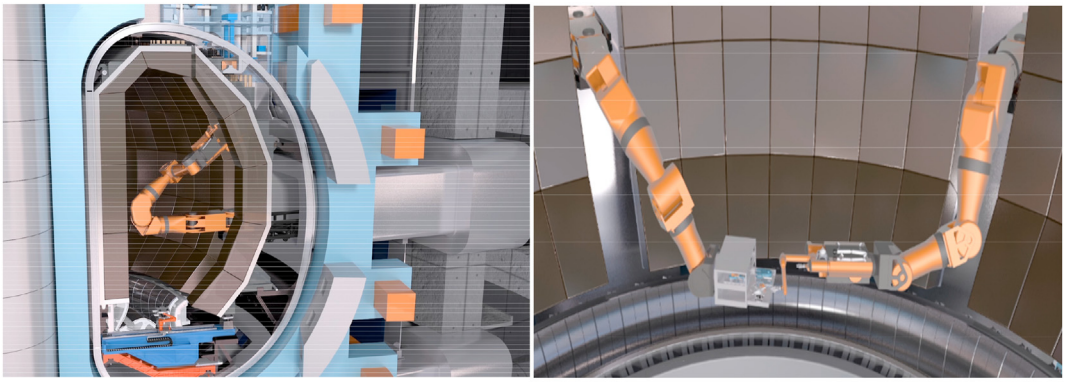

Fig. 1. CMOR work environment; (a) CMOR is used for blanket maintenance operations in vacuum chambers; (b) CMOR dual-arm collaborative operation in a vacuum chamber.

designed controller cannot realize high-precision trajectory tracking, and a nonlinear system identification has to be carried out [10]. The commonly used error identification methods are kinematic calibration and non-kinematic calibration methods [11,12]. The DH parameter error (geometric error) in kinematic modeling is mainly solved by kinematic calibration. However, non-kinematic calibration mainly solves the robot's non-geometric errors, including the flexible deformation of the connecting rods and joints, the variable load at the end, the deformation caused by external force fields. For the CMOR's large load handling applications, the non-geometric factors are among the leading factors affecting the trajectory and positioning accuracy of the robot, so the identification of the CMOR's non-geometric errors is of great practical significance.

At present, the research and application of the CMOR are still in the exploratory stage. The trajectory tracking error of the CMOR's end-effector is relatively large due to the deformation of the flexible joint and flexible rod, and other factorsconclusion is drawn in Section 5. In addition, the CMOR's workspace has a symmetry, and the end-effector position errors under different spatial poses and loads are different, so a single parametric error compensation model cannot be used to compensate for the entire CMOR's moving space. In order to solve these problems, this paper compensates the variable parameter error of the CMOR in a multi-field coupled operating environment based on the principle of the grid-based workspace and the linearized variable load model so as to improve the trajectory tracking accuracy of the CMOR's end-effector.

Considering the above research content, this paper is divided into five chapters. Section 2 describes the CMOR's structure characteristics and establishes dynamic equation. In Section 3, the variable parameter error compensation algorithm is established based on the grid workspace principle and the linearized variable load model. Section 4 establishes a CMOR rigid-flexible coupling model based on the finite element software and uses the Adams-MATLAB/Simulink co-simulation software to conduct a CMOR error analysis and a variable-parameter compensation algorithm verification. Finally, a short conclusion is drawn in Section 5.

2. The model parameters of CMOR

The CMOR can bear ultra-high loads, and it is used for various maintenance operations of in-vessel components. The structure and the coordinate system corresponding to each joint are shown in Fig. 2, the DH parameters are shown in Table 1. Apart from the freedom of the end-effector and the translation of the connecting rod 1, the CMOR has a total of 8° of freedom. Thus, it can flexibly adjust its attitude in the limited vacuum chamber space, move its end-effector to any maintenance site, and complete various maintenance operations. In order to obtain the spatial trajectory tracking

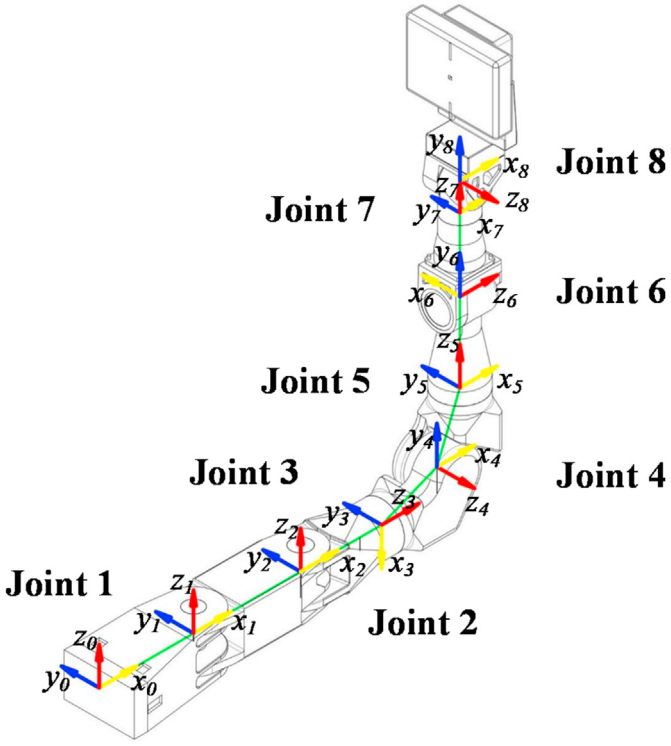

Fig. 2. Coordinate diagram of the CMOR's connecting rod.

Table 1
D-H parameters of the CMOR.

Rod (i)	Variable (θi)	Rotation Angle (°)	Distance (m)	Range (°)
1	$\theta 1$	(0, 0, 0)	(0, 0, 0)	−90~+90°
2	$\theta 2$	(0, 0, 0)	(1.76, 0, 0)	−90~+90°
3	$\theta 3$	(0, 90°, 0)	(0, 0, 1.33)	−180~+180°
4	$\theta 4$	(90°, 0, 90°)	(-0.375, 0.91, 0)	0~+180°
5	$\theta 5$	(−90°, 0, 0)	(0.375, 0, 0.94)	−180~+180°
6	$\theta 6$	(90°, 90°, 0)	(0, 1.3, 0)	−90~+90°
7	$\theta 7$	(−90°, −90°,0)	(0, 1.19,0)	−100~+100°
8	$\theta 8$	(90°, 0, 0)	(0, 0, 0.46)	−90~+90°

performance data of the CMOR's end-effector, it is necessary to establish a CMOR dynamic equation and design a controller for the co-simulation of the rigid and flexible coupling. In this paper, the CMOR's dynamic equation was established using the Lagrange method, and a neural network adaptive sliding mode controller (NNASMC) was established based on the literature [13]. Each bar was processed using the finite element software, and the space trajectory tracking data of the CMOR's rigid-flexible coupling model end-effector was obtained using the Adams-MATLAB/Simulink co-simulation platform [14,15].

2.1. The CMOR's dynamic equation

The CMOR is a typical serial multi-joint mechanical arm. The final dynamic model can be expressed as:

$$\boldsymbol{T}=\boldsymbol{M}(\boldsymbol{q})\ddot{\boldsymbol{q}}+\boldsymbol{H}(\boldsymbol{q},\dot{\boldsymbol{q}})\dot{\boldsymbol{q}}+\boldsymbol{G}(\boldsymbol{q})+\Delta\boldsymbol{R}(\boldsymbol{q},\dot{\boldsymbol{q}})+\Delta\boldsymbol{K}(\boldsymbol{q},\dot{\boldsymbol{q}})+\boldsymbol{D} \tag{1}$$

where $\ddot{\boldsymbol{q}}\in R^8$ is the joint angular acceleration vector, $\dot{\boldsymbol{q}}\in R^8$is the joint velocity vector, $\boldsymbol{T}\in R^8$ is the input torque vector, $\boldsymbol{M}(\boldsymbol{q})\in R^{8\times8}$ is a nonsingular positive definite inertial force matrix, $\boldsymbol{H}(\boldsymbol{q},\dot{\boldsymbol{q}})\dot{\boldsymbol{q}}\in R^{8\times8}$ is the term of the centrifugal force and Coriolis forces, $\boldsymbol{G}(\boldsymbol{q})\in R^8$ is the gravity moment vector (including the connecting rod, rotor, and the moment of gravity of the end-effector), $\Delta\boldsymbol{R}\in R^8$ and $\Delta\boldsymbol{K}\in R^8$ represent the torque variation caused by the flexible deformation of the joints and the connecting rods, and $\mathbf{D}\in R^8$ represents the bounded unknown disturbance of the unbuilt dynamic model.

A variety of controllers can be designed for motion control based on CMOR dynamic equation (Literature [13] NNASMC controller was adopted in this paper), but the deformation error caused by external interference such as non-geometric factors cannot be directly compensated by the controller, and parameter identification is needed.

3. CMOR parameter identification

3.1. CMOR matrix differential error modeling

The parameter error of the robot in the joint space is not evenly distributed due to factors such as the connecting rod flexibility, joint flexibility, dead weight, variable loads, and motor control. For the CMOR, due to the errors in the parameters of each joint, the actual position $\boldsymbol{P^R}\in R^3$ of the center point of the CMOR end effector can be expressed as:

$$\boldsymbol{P^R}=\boldsymbol{F}(\boldsymbol{\theta}+\Delta\boldsymbol{\theta},\boldsymbol{\alpha}+\Delta\boldsymbol{\alpha},\boldsymbol{d}+\Delta\boldsymbol{d},\boldsymbol{a}+\Delta\boldsymbol{a},\boldsymbol{\beta}+\Delta\boldsymbol{\beta}) \tag{2}$$

where $\Delta\boldsymbol{\theta}$ is the joint angular deviation, $\Delta\boldsymbol{\alpha}$ is the joint twist angle deviation, $\Delta\boldsymbol{d}$ is the connecting rod offset, $\Delta\boldsymbol{a}$ is the length deviation of the connecting rod. In order to avoid the singular problem caused by two adjacent axes being parallel to each other, the rotation angle $\boldsymbol{\beta}$ around the $\boldsymbol{y}$ axis is introduced to modify the DH parameter, $\Delta\boldsymbol{\beta}$ is the deviation of the parameter $\boldsymbol{\beta}$ [16].

$$\begin{aligned}\Delta\boldsymbol{P}&=\boldsymbol{P^R}-\boldsymbol{P^N}\\&=\boldsymbol{F}(\boldsymbol{\theta}+\Delta\boldsymbol{\theta},\boldsymbol{\alpha}+\Delta\boldsymbol{\alpha},\boldsymbol{d}+\Delta\boldsymbol{d},\boldsymbol{a}+\Delta\boldsymbol{a},\boldsymbol{\beta}+\Delta\boldsymbol{\beta})-\boldsymbol{F}(\boldsymbol{\theta},\boldsymbol{\alpha},\boldsymbol{d},\boldsymbol{a},\boldsymbol{\beta})\end{aligned} \tag{3}$$

where $\boldsymbol{P^N}\in R^3$ is the theoretical end position, and $\Delta\boldsymbol{P}\in R^3$ is the end position error value. After dropping the high-order perturbation term from the above equation, and introducing multiple sampling points, we can get:

$$\begin{bmatrix}\Delta\boldsymbol{P}_1\\ \Delta\boldsymbol{P}_2\\ \vdots\\ \Delta\boldsymbol{P}_n\end{bmatrix}=\begin{bmatrix}\frac{\partial\boldsymbol{P}_1}{\partial\boldsymbol{\theta}} & \frac{\partial\boldsymbol{P}_1}{\partial\boldsymbol{\alpha}} & \frac{\partial\boldsymbol{P}_1}{\partial\boldsymbol{d}} & \frac{\partial\boldsymbol{P}_1}{\partial\boldsymbol{a}} & \frac{\partial\boldsymbol{P}_1}{\partial\boldsymbol{\beta}}\\ \frac{\partial\boldsymbol{P}_2}{\partial\boldsymbol{\theta}} & \frac{\partial\boldsymbol{P}_2}{\partial\boldsymbol{\alpha}} & \frac{\partial\boldsymbol{P}_2}{\partial\boldsymbol{d}} & \frac{\partial\boldsymbol{P}_2}{\partial\boldsymbol{a}} & \frac{\partial\boldsymbol{P}_2}{\partial\boldsymbol{\beta}}\\ \vdots & \vdots & \vdots & \vdots & \vdots\\ \frac{\partial\boldsymbol{P}_n}{\partial\boldsymbol{\theta}} & \frac{\partial\boldsymbol{P}_n}{\partial\boldsymbol{\alpha}} & \frac{\partial\boldsymbol{P}_n}{\partial\boldsymbol{d}} & \frac{\partial\boldsymbol{P}_n}{\partial\boldsymbol{a}} & \frac{\partial\boldsymbol{P}_n}{\partial\boldsymbol{\beta}}\end{bmatrix}\begin{bmatrix}\Delta\boldsymbol{\theta}\\ \Delta\boldsymbol{\alpha}\\ \Delta\boldsymbol{d}\\ \Delta\boldsymbol{a}\\ \Delta\boldsymbol{\beta}\end{bmatrix}=\boldsymbol{J}\boldsymbol{\eta} \tag{4}$$

where n is the number of sampling points, $\boldsymbol{J}\in R^{n\times5}$ is the parameter error Jacobian matrix, $\boldsymbol{\eta}\in R^5$ is the parameter error matrix.

The parameter error of the CMOR in the joint space varies with the connecting rod flexibility, joint flexibility, control error of the controller, dead weight, and variable loads. With the change in the joint rotation angle in the CMOR's joint space, the joint rotation angle leads to some errors, which are also accompanied by the connecting rod flexibility error and the controller control error. Other parameters will also result in some changes. Therefore, each parameter error of the CMOR can be expressed as a function of the joint angle in the joint space:

$$\boldsymbol{\eta}=[\,\Delta\boldsymbol{\theta}\quad\Delta\boldsymbol{\alpha}\quad\Delta\boldsymbol{a}\quad\Delta\boldsymbol{d}\quad\Delta\boldsymbol{\beta}\,]^T=\boldsymbol{f}(\theta_1,\theta_2\cdots,\theta_8), \tag{5}$$

where $\boldsymbol{\eta}$ represents the set of parameter errors, $\boldsymbol{f}$ represents the function set after all parameter errors $[\,\Delta\boldsymbol{\theta}\quad\Delta\boldsymbol{\alpha}\quad\Delta\boldsymbol{a}\quad\Delta\boldsymbol{d}\quad\Delta\boldsymbol{\beta}\,]$ are all equivalent to the joint angle errors. Since the CMOR joint angles $\theta_1,\theta_2\cdots,\theta_8$ are coupled to each other, it is difficult to establish an error model in the joint space. Therefore, the determined spatial pose in the CMOR joint space can be converted to the working space for a solution as follows.

$$\boldsymbol{\eta}=[\,\Delta\boldsymbol{\theta}\quad\Delta\boldsymbol{\alpha}\quad\Delta\boldsymbol{a}\quad\Delta\boldsymbol{d}\quad\Delta\boldsymbol{\beta}\,]^T=\boldsymbol{g}(x,y,z). \tag{6}$$

where $\boldsymbol{g}$ represents the function set formed by transforming the error function $\boldsymbol{f}(\theta_1,\theta_2\cdots,\theta_8)$ of all joint angles into the working space under the condition of determining the robot's spatial pose.

3.2. CMOR variable parameter error compensation

According to Eq. (5) and Eq. (6), a set of pose parameters in a given workspace can be obtained, and the CMOR's parameter error $\boldsymbol{\eta}$ under that pose can be determined. Due to the large variation in the CMOR's pose in the workspace, the non-geometric factors, such as the connecting rod flexibility, joint flexibility, controller control error, and dead weight under each spatial pose, cause the uneven distribution of the position error space of the end-effector. In addition, the CMOR's terminal is subject to a variable load of 0–2000 kg, which also has a great influence on the position accuracy of the end-effector. Therefore, the ability to improve the absolute position accuracy of the CMOR's end-effector by using a single fixed parameter to compensate for the position error in the whole workspace is limited. In this paper, a CMOR workspace meshed variable parameter error compensation method is proposed, as shown in Fig. 3. Through the grid partition of the workspace, the parameter error $\delta\boldsymbol{\eta_i}$ in each grid was successively identified, so the absolute positioning accuracy of the CMOR's end-effector was improved in the entire workspace.

For a single grid in the CMOR workspace, when the end load is constant, the smaller the grid, the smaller the variation of various parameter errors $[\,\Delta\boldsymbol{\theta}\quad\Delta\boldsymbol{\alpha}\quad\Delta\boldsymbol{a}\quad\Delta\boldsymbol{d}\quad\Delta\boldsymbol{\beta}\,]$. Therefore, in the small range of a single grid, under the premise of sacrificing certain

position accuracy, the constant parameter error set $\boldsymbol{\eta_i} = [\Delta\boldsymbol{\theta_i} \quad \Delta\boldsymbol{\alpha_i} \quad \Delta\boldsymbol{a_i} \quad \Delta\boldsymbol{d_i} \quad \Delta\boldsymbol{\beta_i}]$ of the center point of the grid can be used to compensate the entire grid. When the load changes, in a single grid, the CMOR can be simplified into a linear elastic cantilever structure (ignoring the impact of random errors), so the position error at the end can be equivalent to:

$$\Delta\boldsymbol{p} = \boldsymbol{k}mg + \Delta\boldsymbol{p}^0, \tag{7}$$

where $\Delta\boldsymbol{p}$ is the spatial position error, $\boldsymbol{k}$ is the load position error coefficient, and $\Delta\boldsymbol{p}^0$ is the spatial position error under zero load.

Similarly, a set of parameter error matrices under variable loads in the joint space can be obtained as

$$\boldsymbol{\eta_i^m} = \boldsymbol{k}'mg + \boldsymbol{\eta_i^0} \tag{8}$$

where $\boldsymbol{\eta_i^m}$ is the angular parameter error matrices in the joint space under variable loads, $\boldsymbol{k}'$ is the load joint angle error coefficient, and $\boldsymbol{\eta_i^0}$ is the angle parameter error under zero load.

According to the above analysis, the smaller the single CMOR grid, the less it is affected by the non-geometric factors, such as the connecting rod flexibility, joint flexibility, controller control error, and dead weight. Also, the higher the structural similarity of the CMOR's linear elastic cantilever beam in a single grid, the higher the compensation accuracy of the variable parameters in the whole workspace.

3.3. CMOR parameter error solving process

In this paper, the Levenberg-Marquardt (LM) algorithm of the nonlinear damped least-squares algorithm is used to solve the CMOR parameter error. The LM algorithm is one of the most widely used optimization algorithms, and its ultimate goal is to find a set of parameters that make the function have the minimum parameter vector. In comparison with the Gaussian Newton method and the gradient descent method, the LM algorithm not only has global search and fast optimization abilities in comparison with the gradient descent method, but it also has a faster convergence ability than the Gaussian Newton method in reaching the optimal solution. In addition, it has a unique advantage in dealing with redundant parameters, as it can effectively avoid falling into local optima when solving parameters, and it is also highly efficient in dealing with complex problems [17].

The iterative formula of the Gauss-Newton method is:

$$x^{k+1} = x^k + h_{gn}, \tag{9}$$

$$x^{k+1} = x^k - H^{-1}\nabla f, \tag{10}$$

where ∇f is the Jacobian matrix, H is the Hesse matrix, and the iterative step length is obtained after the simplification:

$$h_{gn} = -\left(J_r^T J_r\right)^{-1} J_r^T J_r \tag{11}$$

Mainly, the LM algorithm is an improvement of the Gauss-Newton method, with a slight difference in iterative step length:

$$h_{gn} = -\left(J_r^T J_r + \mu I\right)^{-1} J_r^T J_r \tag{12}$$

According to the specific structure of the CMOR, the Jacobian matrix and the other parameters are initialized: Set iteration termination condition: $\varepsilon = 0.0001$, set the initial coefficient of the LM iteration algorithm as: $\alpha_1 = 500$, $m = 0.01$, $p_0 = 0.05$, $p_1 = 0.5$, $p_2 = 0.9$, $\lambda_0 = 0.05$ and $k = 1$.

Set the objective function of LM algorithm iteration as:

$$\Delta\boldsymbol{\eta_k} = -\left(J^T(\boldsymbol{\eta_k})J(\boldsymbol{\eta_k}) + \lambda_k \boldsymbol{I}\right)^{-1} J^T(\boldsymbol{\eta_k})\Delta\boldsymbol{P}(\boldsymbol{\eta_k}), \tag{13}$$

where k is the number of iterations, $\Delta\boldsymbol{\eta_k}$ is the parameter error change value at the k-th iteration, $\boldsymbol{\eta_k}$ is the parameter error at the k-th iteration, and λ_k is the damping factor at the k-th iteration.

The iteration termination condition is: the number of iterations is greater than 50 or the parameter error change value at the k-th iteration $\|\Delta\boldsymbol{\eta_k}\| < \varepsilon$.

Each iteration of the LM algorithm includes 5 steps.

Step 1. Establish the deviation function according to $\Delta\boldsymbol{P} = \boldsymbol{P^R} - \boldsymbol{P^N} = \boldsymbol{J}\boldsymbol{\eta}$, where $\Delta\boldsymbol{P}$ is the deviation of the terminal space position, $\boldsymbol{P^R}$ is the actual position, $\boldsymbol{P^N}$ is the calculated position, $\boldsymbol{J}$ is the Jacobian matrix, and $\boldsymbol{\eta}$ is the parameter error vector to be solved.

Step 2. Initialize the Jacobian matrix and the other parameters according to the specific CMOR structure, determine the optimal initial value $\boldsymbol{\eta}$, and terminate the control constant $\varepsilon \geq 0$. Then, according to the initial value $\boldsymbol{\eta}$, calculate the current spatial position error $\Delta\boldsymbol{P}$ at the k-th iteration.

Step 3. Calculate the Jacobian matrix $J(\boldsymbol{\eta_k})$ for the k-th iteration according to the k-th estimate and then use the damped least-square method to solve the parameter error change matrix:

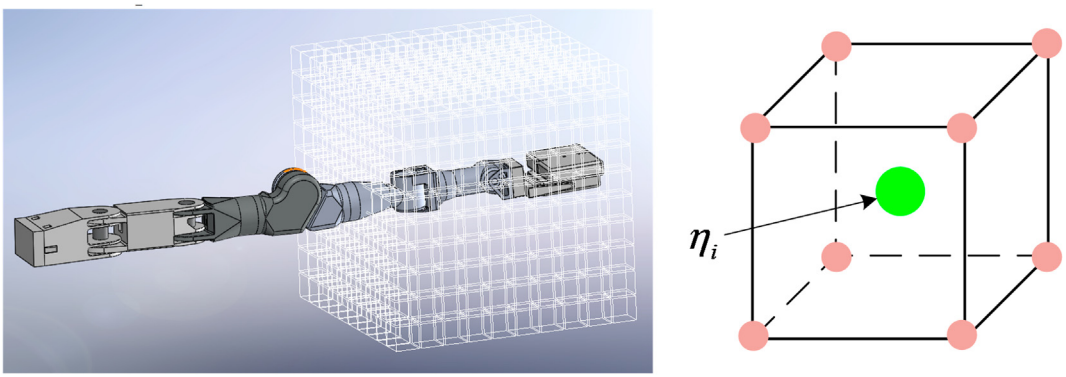

Fig. 3. Principle of the CMOR's meshed workspace.

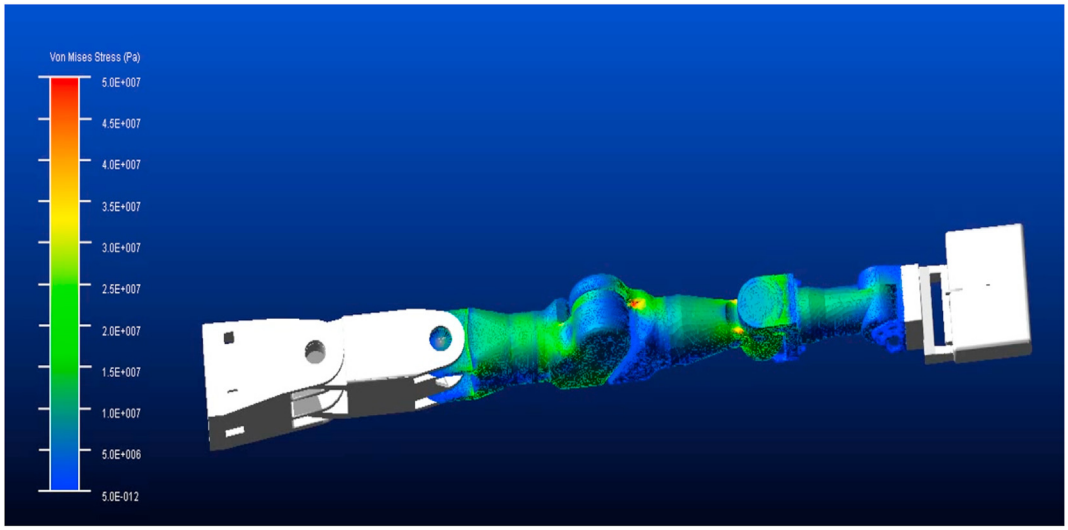

Fig. 4. The CMOR's rigid-flexible coupling model.

$$\Delta\boldsymbol{\eta_k} = -\left(J^T(\boldsymbol{\eta_k})J(\boldsymbol{\eta_k}) + \lambda_k \boldsymbol{I}\right)^{-1} J^T(\boldsymbol{\eta_k})\Delta\boldsymbol{P}(\boldsymbol{\eta_k}), \tag{14}$$

where k is the number of iterations, $\Delta\boldsymbol{\eta_k}$ is the parameter error change value at the k-th iteration, $\boldsymbol{\eta_k}$ is the parameter error at the k-th iteration, and λ_k is the damping factor at the k-th iteration.

$$\lambda_k = \alpha_k\left(\rho\|\Delta\boldsymbol{P_k}\| + (1-\rho)\left\|J_k^T\Delta\boldsymbol{P_k}\right\|\right), \tag{15}$$

The CMOR's current space position error in the $(k+1)$-th iteration after updating the parameter error matrix is calculated as:

$$\Delta\boldsymbol{P}(\boldsymbol{\eta_k} + \Delta\boldsymbol{\eta_k}) = \boldsymbol{P^R} - \boldsymbol{P^N}(\boldsymbol{\eta_k} + \Delta\boldsymbol{\eta_k}) \tag{16}$$

The ratio q_k of the actual drop quantity ΔF_K and the estimated drop quantity ΔL_K at the k-th iteration is calculated to monitor the quality of the step length:

$$\Delta F_K = \|\Delta\boldsymbol{P_k}\|^2 - \|\Delta\boldsymbol{P}(\boldsymbol{\eta_k} + \Delta\boldsymbol{\eta_k})\|^2, \tag{17}$$

$$\Delta L_K = \|\Delta\boldsymbol{P_k}\|^2 - \left\|\Delta\boldsymbol{P_k} + \boldsymbol{J_k^T}\Delta\boldsymbol{\eta_k}\right\|^2, \tag{15}$$

$$q_k = \frac{\Delta F_K}{\Delta L_K}. \tag{18}$$

Step 4. Update the iteration parameters.

The estimated drop amount $\Delta L_K > 0$ is artificially constructed, so if q_k is small or negative, it indicates the failure of the iteration. At this point, $\boldsymbol{\eta_k} + \Delta\boldsymbol{\eta_k}$ cannot be used as the next iteration point. The damping factor λ_k must be increased and the step size $\boldsymbol{\eta_k} + \Delta\boldsymbol{\eta_k}$ must be decreased. The solution is resolved so that the next iteration is closer to the gradient descent method and that the global search is realized. If q_k is large, the iteration is effective. Then, the damping factor λ_k can be reduced and the step size $\boldsymbol{\eta_k} + \Delta\boldsymbol{\eta_k}$ can be increased so that the algorithm is closer to the Gauss-Newton algorithm, which is necessary to achieve a rapid convergence to the optimal solution in the next iteration. In the other cases, the damping factor λ_k and the iteration step size remain the same. Thus, the k-th iteration parameter update rule can be obtained.

The $(k+1)$-th parameter error matrix update is

$$\boldsymbol{\eta_{k+1}} = \begin{cases} \boldsymbol{\eta_k} + \Delta\boldsymbol{\eta_k} & if \;\; r_k > p_0 \\ \boldsymbol{\eta_k} & else \end{cases} \tag{19}$$

The $(k+1)$-th damping factor update rule is

$$\alpha_{k+1} = \begin{cases} 4\alpha_k & if \;\; q_k < p_1 \\ \alpha_k & if \;\; p_1 < q_k < p_2 \\ \max\left\{\frac{\alpha_k}{4}, m\right\} & else \end{cases}. \tag{20}$$

$$k = k + 1. \tag{21}$$

Step 5. When $\left\|J_k^T\Delta\boldsymbol{P_k} < \varepsilon\right\|$ (generally taking $\varepsilon = 0.0001$, the error norm is very close and has already converged) or when the number of iterations reaches 50, the loop is completed, and the parameter error is calculated.

4. Co-simulation results and discussion

In order to verify the trajectory tracking accuracy of the CMOR's rigid-flexible coupling model and the effect of the LM variable parameter error compensation algorithm, the neural network adaptive sliding mode controller (NNASMC) in literature [13] was modeled using MATLAB/Simulink. The CMOR's 3D dynamic model was established using ADAMS software, and the finite element software was used to carry out the flexible processing of the CMOR's connecting rod to realize the co-simulation of the rigid and flexible coupling [18]. The first two connecting rods of the CMOR were made of steel with small deformation, while the rest of the connecting rods were made of aluminum alloy with large deformation. The elastic modulus and Poisson's ratio of all the aluminum alloy connecting rods were set at 70 Gpa and 0.3, respectively, and the flexible processing results are shown in Fig. 4.

4.1. CMOR joint 4 limit pose experiment

In this section, the maximum load under the forward and backward motion of the CMOR and the rigid-flexible coupling deformation error under the limit poses are analyzed. The

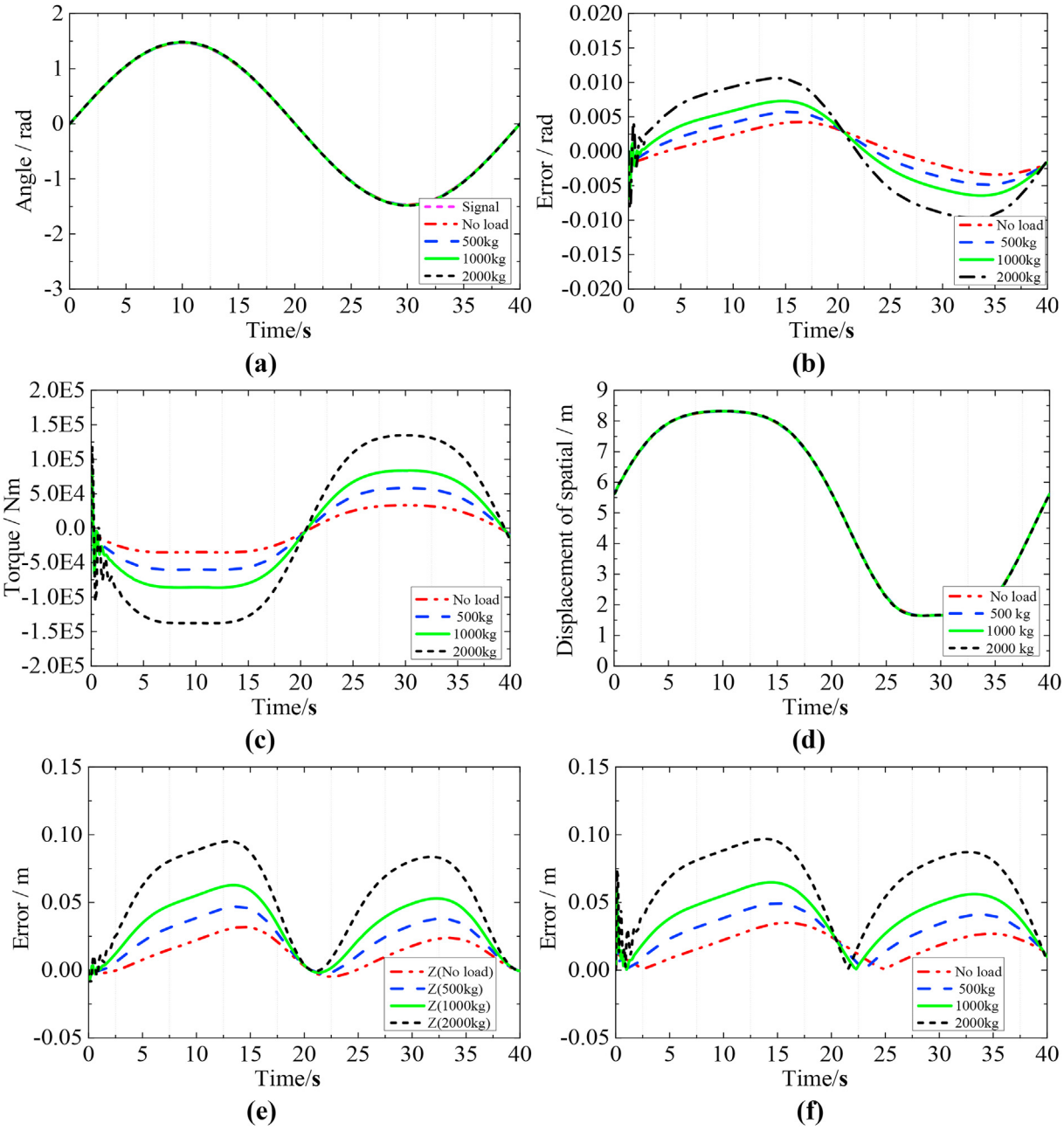

Fig. 5. CMOR flexible model simulation results of the NNASMC controller (Joint 4); (a) Joint angular displacement; (b) Joint angular displacement error; (c) Joint driving torque; (d) Terminal space curve; (e) Terminal Z-axis position error; (f) Terminal space position error.

Table 2
Compensation value of joint 4 at different spatial positions (rad).

Location	1	2	3	4	5	6	7	8
Load(2000 kg)	-1.18×10^{-2}	-1.85×10^{-2}	-2.16×10^{-2}	-1.89×10^{-2}	8.7×10^{-3}	1.66×10^{-2}	1.96×10^{-2}	1.57×10^{-2}
Load(1000 kg)	-6.2×10^{-3}	-1.10×10^{-2}	-1.41×10^{-2}	-1.33×10^{-2}	3.7×10^{-3}	9.5×10^{-3}	1.25×10^{-2}	1.07×10^{-2}
Load(500 kg)	-3.4×10^{-3}	-7.2×10^{-3}	-1.03×10^{-2}	-1.05×10^{-2}	1.3×10^{-3}	5.9×10^{-3}	8.9×10^{-3}	8.2×10^{-3}
No load	-7.08×10^{-4}	-3.6×10^{-3}	-6.7×10^{-3}	-7.8×10^{-3}	-1.1×10^{-3}	2.5×10^{-3}	5.4×10^{-3}	5.8×10^{-3}

sinusoidal movement driving signal of joint 4 was set as shown in Fig. 5a so that the CMOR could rotate forward and backward to the limit poses, and the simulation results are shown in Fig. 5.

(1) CMOR rigid-Flexible coupling control effect

Given the sinusoidal control signal of joint 4, different loads of the end-effector were set (0–2000 kg) to simulate the control

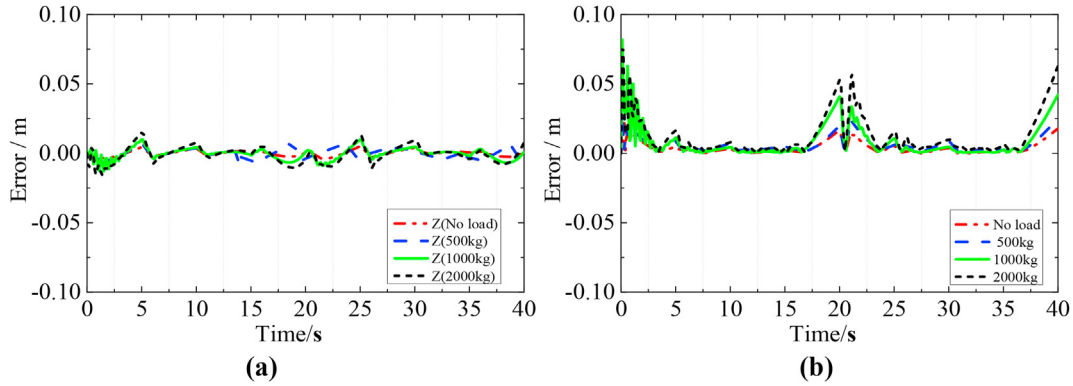

Fig. 6. CMOR trajectory tracking error compensation results based on the LM space grid and the linearized variable load algorithm (Joint 4); (a) Terminal Z-axis position error; (b) Terminal space position error.

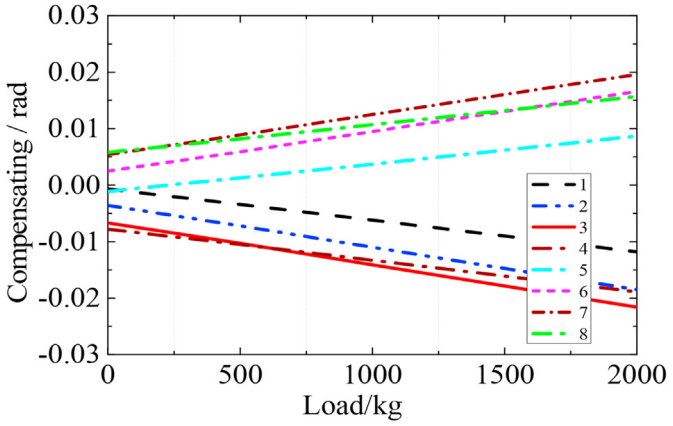

Fig. 7. Linearized compensation parameters of joint 4 under variable loads.

performance of the NNASMC controller, and the results are shown in Fig. 7. The analysis results show that the maximum tracking error of the angular displacement of the joint was about 0.01 rad and that the maximum position error of the end-effector along the Z-axis was about 0.1 m. Also, the spatial position error of the end-effector was similar to the Z-axis position error. It can be seen that the position error of the end-effector was mainly caused by the Z-axis position error caused by the gravity of the CMOR's flexible connecting rod and the end load. Overall, the proposed NNASMC controller has better control performance and less end position error.

(2) Variable parameter position error compensation

The CMOR's workspace was evenly divided into 8 parts along the Y-axis of the base coordinate system, and the LM algorithm space grid and the linearized variable load model were used for the variable parameter error compensation. The compensation parameters in each grid joint space under different end loads are shown in Table 2. The compensation parameters were brought into the NNASMC controller for re-simulation, and the results are shown in Fig. 6. After the compensation, the CMOR position error along the Z end was less than 0.017 m, and the mean value of the space position error was less than 0.02 m. Thus, the end position error was reduced by more than 5 times. In Fig. 6b, the large position errors of 0 s and 20 s were mainly caused by the large variation of the error value in this region and the relatively sparse grid workspace, which can further refine the grid and improve the position accuracy.

4.2. CMOR linearized variable load variable parameter compensation

The parameter error compensation values of the different loads in the same spatial grid were plotted as curves, as shown in Fig. 7. The parameter error compensation values of the same space grid under different loads are linearly related to the loads, and the position error compensation value under various load values can be obtained by calculating the slope.

5. Conclusion

In this paper, by using ADAMS and MATLAB/Simulink, the trajectory tracking error of the CMOR's rigid-flexible coupling model was analyzed. The results showed that the position error of the CMOR's rigid-flexible coupling model exceeded 0.1 m in the extreme posture. In order to compensate for the position error, this paper proposed a variable parameter error compensation algorithm for the CMOR workspace based on the LM nonlinear damped least-square method, the spatial grid, and the linearized variable load principle. The effect of the trajectory tracking error compensation was verified by joint simulation, and the results showed that the variable parameter error compensation algorithm significantly reduced the trajectory tracking error under the CMOR limit position, where the position error was less than 0.02 m. Overall, the proposed method in this study provides a reference for the research of the position error compensation of rigid-flexible coupling models.

In the future, combined with the existing trajectory tracking position error compensation algorithm, we aim to explore and investigate an adaptive mesh density compensation algorithm with variable mesh sizes so as to improve the regional compensation effect due to which the CMOR error value greatly varies. The developed error compensation algorithm can also be used in other fields.

Declaration of competing interest

The authors declare that they have no known competing financial interests or personal relationships that could have appeared to influence the work reported in this paper.

Acknowledgments

This work was supported by the National Natural Science Foundation of China (Grant Nos. 11802305, 51875281, and 51861135306), the China National Special Project for Magnetic

Confinement Fusion Science Program (Grant No. 2017YFE0300503), and the Fundamental Research Funds for the Central Universities (Grant No. NP2018112).

Appendix A. Supplementary data

Supplementary data to this article can be found online at https://doi.org/10.1016/j.net.2021.02.005.

References

[1] M. Lei, Y. Song, S. Liu, et al., Conceptual design of the HCCB blanket system integration for CFETR, Int. J. Energy Res. 43 (2019) 3306–3312.
[2] C. Choi, A. Tesini, R. Subramanian, et al., Multi-purpose deployer for ITER in-vessel maintenance, Fusion Eng. Des. 98–99 (2015) 1448–1452.
[3] H. Tian, D. Zhao, F. Yin, et al., Kinematic calibration of a 6-DOF hybrid robot by considering multicollinearity in the identification Jacobian, Mech. Mach. Theor. 131 (2019) 371–384.
[4] A. Cibicik, E. Pedersen, O. Egeland, Dynamics of luffing motion of a flexible knuckle boom crane actuated by hydraulic cylinders, Mech. Mach. Theor. 43 (2020) 1–18.
[5] N. Liu, X. Zhang, L. Zhang, et al., Study on the rigid-flexible coupling dynamics of welding robot, Wireless Pers. Commun. 102 (2018) 1–12.
[6] M.S. Manuelraj, P. Dutta, K.K. Gotewal, et al., Structural analysis of ITER multi-purpose deployer, Fusion Eng. Des. 109 (2016) 1296–1301.
[7] G.G. Sen, S. Mukhopadhyay, M. Chris H, et al., Master slave control of a tele-operated anthropomorphic robotic arm with gripping force sensing, IEEE. T. Instrum. Meas. 55 (2006) 2136–2145.
[8] L. Huang, Y. Hironao, N. Tao, et al., A master–slave control method with gravity compensation for a hydraulic teleoperation construction robot, Adv. Mech. Eng. 9 (2017) 1–11.
[9] B. Haist, S. Mills, A. Loving, Remote handling preparations for JET EP2 shut-down, Fusion Eng. Des. 84 (2–6) (2009) 875–879.
[10] G. Liu, X. Wu, Y. Chen, et al., Analysis of influences of end position mass and joint rotary inertia on motion stability of a flexible manipulator arm, China Mech. Eng. 25 (4) (2014) 480–485.
[11] Y. Zhang, C. Liu, P. Liu, Industrial robot kinematics parameter identification, Adv. Mater. 889 (2014) 1136–1143.
[12] X. Shan, G. Cheng, Structural error and friction compensation control of a 2(3PUS+S) parallel manipulator, Mech. Mach. Theor. 124 (2018) 92–103.
[13] G. Qin, A. Ji, W. Wang, et al., Analyzing trajectory tracking accuracy of a flexible multi-purpose deployer, Fusion Eng. Des. 151 (2020) 1–10.
[14] L. Yan, W. Xu, Z. Hu, et al., Virtual-base modeling and coordinated control of a dual-arm space robot for target capturing and manipulation, Multibody Syst. Dyn. 45 (2018) 431–455.
[15] H. Luo, Y. Liu, Z. Chen, et al., Co-simulation control of robot arm dynamics in ADAMS and MATLAB, Res. J. Appl. Sci. Eng. Technol. 6 (20) (2013) 3778–3783.
[16] S. Hayati, M. Mirmirani, Improving the absolute positioning accuracy of robot manipulators, J. Rob. Syst. 2 (4) (1985) 397–413.
[17] P. Hong, W. Tian, D. Mei, et al., Robotic variable parameter accuracy compensation using space grid, Robot 37 (3) (2015) 327–335.
[18] C. Zhang, Dynamic modeling of robot arm with joint and link flexibility manipulating a constrained object, Chin. J. Mech. Eng-En. 39 (6) (2013) 9–12.